POLITECNICO
MILANO 1863

SCUOLA DI INGEGNERIA INDUSTRIALE
E DELL'INFORMAZIONE

Executive Summary of the Thesis

Ejecta plume observability from an asteroid small impactor mission

Laurea Magistrale in Space Engineering - Ingegneria Spaziale

Author: Pierpaolo Merola

Advisor: Prof. Camilla Colombo

Co-advisor: Mirko Trisolini

Academic year: 2021-2022

1. Introduction

Asteroids have always been a subject of study for understanding the formation of the solar system, as well as the appearance of life on our planet. NEOs are the most attractive targets for robotic probes, guaranteeing a lower cost and the possibility of maintaining mission control from ground stations. A particular method of asteroid composition study is the observation of the crater and the ejecta dust deriving from the impact on its surface. This method is complementary to simple asteroid observation and allows for the creation of more sophisticated dynamics models in a low-gravity environment. The aim of this research is the ejecta plume observability characterization of small impact on the asteroid's surface, using a simulated image generator developed specifically for this study. The asteroid 162173 Ryugu is the main subject of the research, and the impact on its surface has the characteristics of the one that already occurred in the Hayabusa2 mission, to have a direct comparison with the real images.

2. Dynamics model

For the propagation of dust particle dynamics, Circular Restricted Three Body Problem (CR3BP) is used, from which it is possible to obtain closed-form solutions. The nondimensional photo-gravitational CR3BP formulation simplify equations of motion, already amply investigated in the work of Latino [9]. The development of the model with respect to the study just mentioned is the use of the gravitational field coefficient J_4. As reported in Kikuchi et al. [5], Ryugu exhibits a strong zonal gravitational force associated with the J_4 term, due to its spinning-top shape. For clarity of wording and nomenclature, the dimensionless values are reported in lowercase letters. In Figure 1 is shown the Sun-asteroid synodic reference system used for the dimensionless equations of motion derivation, where r_{sp} is the Sun - particle adimensional distance, and r_{ap} is the asteroid - particle adimensional distance.

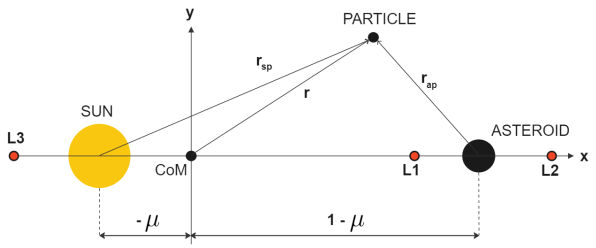

Figure 1: Sun - asteroid synodic reference frame with adimensional values.

The first step is to calculate the adimensional mass parameter μ to model the system where the investigated dust will transit:

$$\mu = \frac{m_a}{m_s - m_a} \tag{1}$$

Solar radiation contributes as acceleration, which must be included in the equations of motion. The Cannonball model is used, where a spherical object with the same optical properties is affected by the SRP However, it is more convenient to insert it into the equations as the ratio between the SRP acceleration and the gravitational acceleration of the Sun. In this way, the lightness parameter β is obtained [9]:

$$\beta = \frac{P_0}{c}\frac{r_{es}^2}{\mu_{sun}}\frac{3}{2\rho_p d}c_R \tag{2}$$

Where the solar flux $P_0 = 1367$ W/m^2 is taken at 1 AU away from the Sun, c is the speed of light and r_{es} is the Sun-Asteroid distance. The reflectivity coefficient is set to $c_R = 2$, corresponding to an ideal specular reflection, and the density ρ_p is set equal to the mean density of Ryugu [13]. The presence of the particle diameter d in the denominator indicates that the effect of solar radiation changes depending on the size of the hit particles. The resulting equations of motion are written in compact form:

$$\begin{cases} \ddot{x} - 2\bar{n}\dot{y} = V_{/x} \\ \ddot{y} + 2\bar{n}\dot{x} = V_{/y} \\ \ddot{z} = V_{/z} \end{cases} \tag{3}$$

Where $\bar{n}$ is the mean motion, and the potential V is the sum of the gravitational contribution of the two primaries, the rotating system contribution, and the solar radiation contribution:

$$\begin{aligned} V = {} & \frac{1}{2}(x^2+y^2) + \frac{(1-\beta)(1-\mu)}{r_{sp}} + \frac{\mu}{r_{ap}} + \\ & - \frac{\mu}{r_{ap}} J_2 \left(\frac{R}{r_{ap}}\right)^2 \frac{1}{2}\left(3\left(\frac{z}{r_{ap}}\right)^2 - 1\right) + \\ & - \frac{\mu}{r_{ap}} J_4 \left(\frac{R}{r_{ap}}\right)^4 \frac{1}{8}\left(35\left(\frac{z}{r_{ap}}\right)^4 + \right. \\ & \left. - 30\left(\frac{z}{r_{ap}}\right)^2 + 3\right) \end{aligned} \tag{4}$$

3. Initial conditions

In order to use the data obtained from the laboratory tests it was necessary to implement an ejecta scaling law, with the point source approximation of the projectile impacting, which is a good approximation for hypervelocity impacts, as in the work of Housen & Holsapple model [3], from which the crater formation model is taken to set the initial conditions. The impact crater radius is obtained as follows (with all the parameters referred to the case of impact under gravity regime, due to the Ryugu composition [13]):

$$R_c = H_1 \left(\frac{\rho}{\delta}\right)^{\frac{2+\mu-6\nu}{6+3\mu}} \left(\frac{ga}{U^2}\right)^{-\frac{\mu}{2+\mu}} \left(\frac{\rho}{m}\right)^{-\frac{1}{3}} \tag{5}$$

It is therefore possible to obtain the speed as a function of the distance from the point of impact x up to R_c:

$$u_p = C_1 U \left(\frac{x}{a}\left(\frac{\rho}{\delta}\right)^{\nu}\right)^{-\frac{1}{\mu}} \tag{6}$$

In this way, the ejecta velocity is applied to the particle with a given orientation (always taken radial with respect to the center of impact) and an inclination that is a monotonic function with respect to the distance from the impact location, as reported in Richardson et al. [10]. Also the rotation of the asteroid is considered to set the initial conditions of each individual particle. Particle size is the only parameter in the literature that is not linked to any other impact-related variable, and this study is limited to the sizing of powders with a cumulative distribution function [6], with the slope exponent of the power law set equal to 2.7.

4. Image simulation model

The developed optical system is based on a simple pinhole model, that was chosen due to the already proven efficiency of the reference camera for the observation of the event. Besides, the observation location at the impact moment is essential for safety and for obtaining useful images. Studies of this kind have been addressed, especially for the safety and for the collectability of dust directly in orbit around the asteroid, as in the work of Trisolini et al. [11]. To obtain the ejecta dust images, three conditions are necessary to evaluate the visibility of dust particles:

the particle must be within the camera's field of view (FoV); the particle must not be in eclipse with respect to the Sun; the particle must not be in eclipse with respect to the camera.
To obtain the solar radiation reflected towards the observer by the particles, the phase angle ϕ and scattering computations are necessary. The phase angle varies from 0 to 180 degrees, but the Sun in the field of view is avoided. Two different models for the solar flux radiated by the particles have been implemented. The first one, developed by Hergenrother et al.[2] for the study of the ejecta dust of the asteroid (101955) Bennu, has been applied to obtain Dart impact simulated images, as seen in Fahnestock et al. [1], valid only for a phase angle value between 70° and 120° of phase angle. The second model, the Lambertian (diffusely-reflecting) sphere model, is used to compute the reflected solar radiation with the expression derived by Vallerie [12]. A possible third model is obtained by combining the two models and creating a continuous function, in which the Hergenrother model is assumed only in its range of validity.

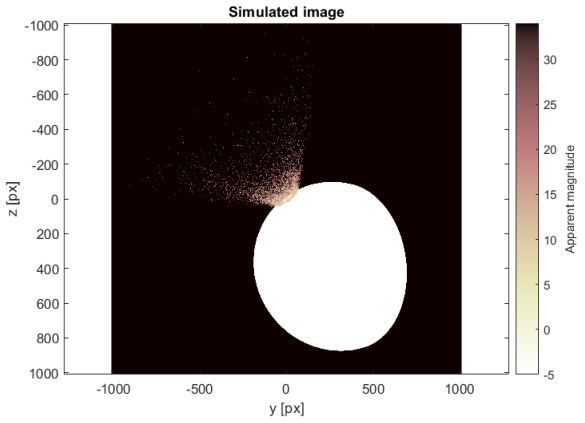

Figure 2: Impact view form camera at [-1,-1,0] km asteroid centre synodic reference frame, impact pointing.

The studies conducted on the DCAM3-D reference camera help to understand the entity of the diffraction, to model the point spread function (PSF). In particular, a gaussian distribution of the irradiation that hits the single pixels is implemented. With different standard deviation σ values, the irradiation is more or less distributed on the adjacent pixels. To evaluate the sigma value, a dust particle placed 1 km away from the observer with a phase angle of 90 degrees is used. From the images obtained by the DCAM3 camera [4] from Hayabusa2 probe, the comparison with the images of the light source led to the σ selection equal to 0.2. The asteroid visualization is modeled as a spherical body with a homogeneous constant reflection of sunlight which depends exclusively on the albedo. An example can be seen in Figure 2, with a random impact on the sunlit surface of the asteroid. The image is simulated 20 minutes after the impact at 45 degrees latitude, on the sunlit side of the asteroid.

5. Nanolander for images comparison

The use of a lander on the asteroid's surface at the impact moment has been previously explored as part of the AIDA program, with the MASCOT2 nanolander intended for deployment during the Dart impact on the Dimorphos asteroid [7]. Unfortunately, the nanolander was ultimately not utilized. In the Hayabusa2 mission, the MASCOT nanolander was successfully deployed on the surface of asteroid Ryugu with the aim of conducting on-site surface studies [8]. In this thesis, the lander is studied for direct ejecta plume observation, a different purpose than MASCOT and MASCOT2, which are used as references for this study anyway. With new mission tasks, new requirements are needed:

- The lander's solar arrays and secondary battery are expected to provide an operational lifetime of more than 3 months.
- The extension of the solar panels shall take place for each stationing on the surface and be retracted for a programmed displacement or for the imminent approach of the dust particles generated by the impact.
- The lander shall be positioned at a sufficient distance from impact to guarantee its safety.
- The lander shall have implemented a seismograph capable of detecting the seismic waves.

For positioning the lander at a safe distance, the uncertainty of the impact location must be considered [8]. The position of the landers is chosen 20 crater radii from the uncertainty zone, and the images will be obtained for a maximum time of 45 minutes after the impact, to avoid damages due to the ejecta dust. If the impact does not

occur at the designated point, a reduction of the image acquisition time may be necessary.

6. Results

The simulated images presented and studied in this chapter are used to develop a model for asteroid impact observability, attempting to understand the effects of reflected sunlight and the properties of detectable dust. The comparison between the simulated images and the real images from the DCAM3 camera during the Hayabusa2 mission is performed. From Figure 3 to Figure 4 the comparisons at 100 and 192 seconds after the impact are shown in sequence. The simulated images are obtained from the observer position [-0.5 -0.5 0,3] km (synodic reference system centered on the asteroid), and a scale bar is inserted, as in the real images, to get an idea of the size of the ejecta cone. The scale bar is representative of the impact point.

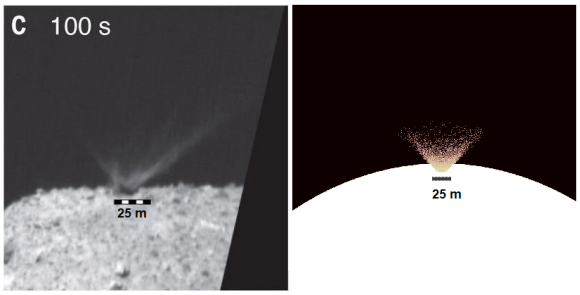

Figure 3: Simulated image (right figure) - real image (left figure) comparison at 100 seconds after impact.

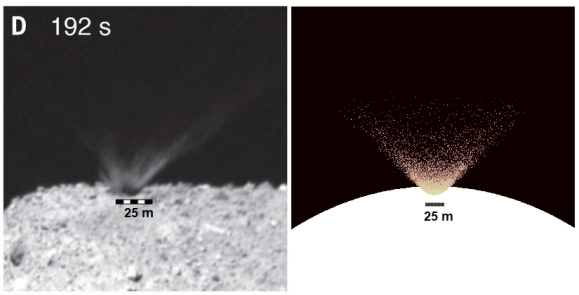

Figure 4: Simulated image (right figure) - real image (left figure) comparison at 192 seconds after impact.

As far as the dimensions of the cone are concerned, the images are superimposable in all time instants studied, even if the tips of the dust branches reach greater distances than those of the simulations. The visualization of the shape and deformation of the ejecta cone is visualized in the Figure 5 and Figure 6.

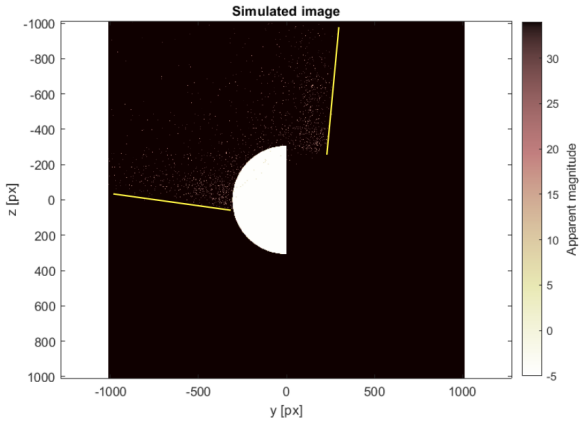

Figure 5: 45° latitude - 180° longitude impact. Particle size of 0.1 mm with cone edge line.

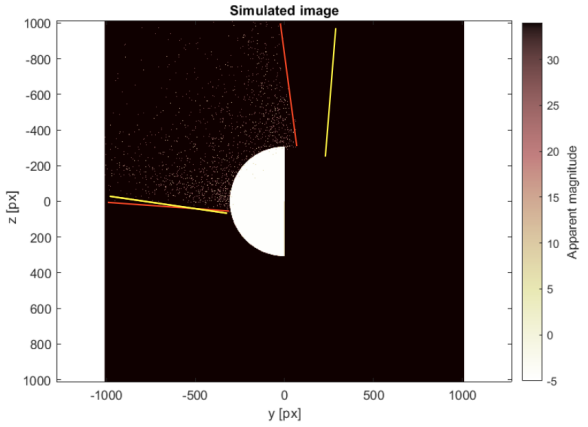

Figure 6: 45° latitude - 180° longitude impact. Particle size of 1 mm with cone edge line of 0.1 mm and 1 mm size cone.

In Figure 5, the 2 edges of the 0.1 mm particle size ejecta cone are marked in yellow. The images are taken 30 minutes after impact at [0,-2,0] km observer location. In Figure 6 the same support lines (in red), are applied to the 1 mm particle size ejecta cone, with those of the previous figure for a more effective comparison. It is evident how the two structures at the same instant of time are different. The computed distance between different particles is not accurate, due to the perspective error. The proximity to the event does not allow for accurately visualize the edges of the cone, therefore the data must be compared with the dynamic model and with multiple observations. With the use of image resolution data and knowing the observer-

asteroid distance, it is possible to approximately compute the difference in position between 0.1 and 1 mm particle sizes, which can reach over 260 meters after 30 minutes in the antisolar direction.
The study on the various photometric models implemented has brought different levels of magnitude as results: the first model mentioned in Section 4 generates images with a smaller magnitude than the second mentioned. furthermore, the study of the magnitude over time is evaluated. Figure 6.18 shows the trends of the average magnitude calculated on the images between 5 and 80 minutes after the impact for three different observer locations. In the first ejecta cone growth phase, the magnitude decreases, although dust dispersion increases the magnitude per pixel. The closer the observer is to the event, the sooner the maximum perceived brightness is reached, with a higher brightness peak at greater distances. It is important to remember that the reported value is indicative only for the comparison between the cases, and not as a reference value of brightness acquired from the image.

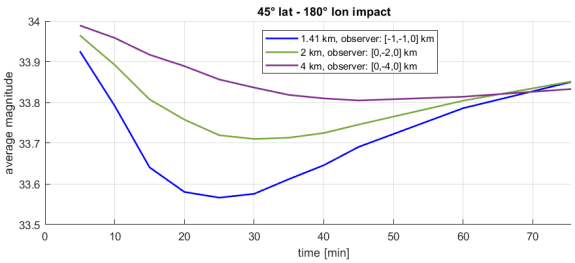

Figure 7: Average magnitude over time of the same impact from three different observer location: [-1,-1,0] km in blue, [0,-2,0] km in green, [0,-4,0] km in violet.

Finally, some of the images obtainable from the nanolander are reported with different impact locations due to uncertainty. It is evident that the visibility increases with an impact closer to the lander. Furthermore, a 60° FoV camera is implemented to understand its usefulness. The camera parameters are the same as MASCAM, the camera used in the MASCOT lander. As seen in Figure 9, with a 60° FoV camera, 45 minutes after impact, the time limit established for observation for lander safety, the sides of the cone are clearly visible.

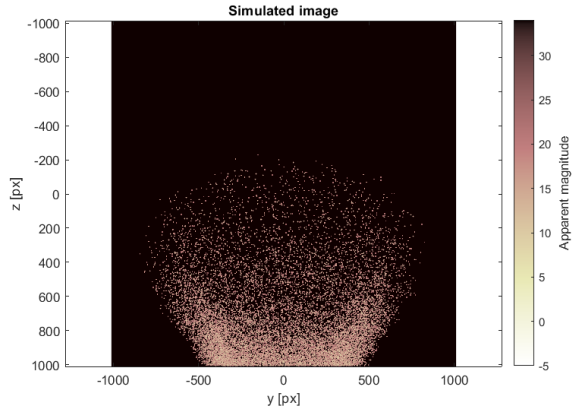

Figure 8: Lander simulated images at 10 minutes after impact at edge of uncertainty area.

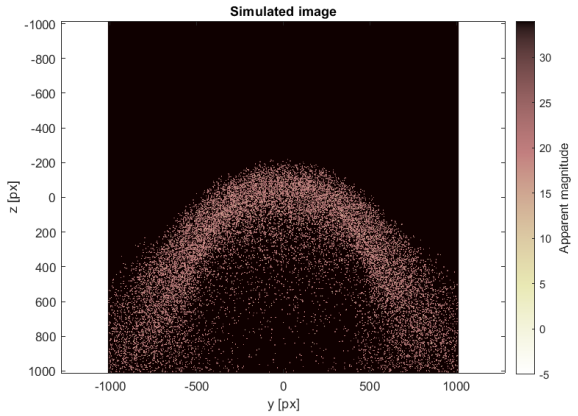

Figure 9: Lander simulated image at 45 minutes after impact at the established point. 60° FoV camera.

In the end, a comparison between the lander and spacecraft images at the same instant time is shown in Figure 10 and 11.

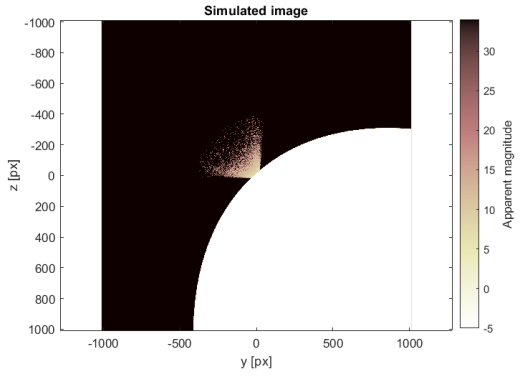

Figure 10: Spacecraft impact simulated image at camera position [-0.5, -0.5, 0] km. Impact at 45° latitude and 180° longitude, 5 minutes after impact.

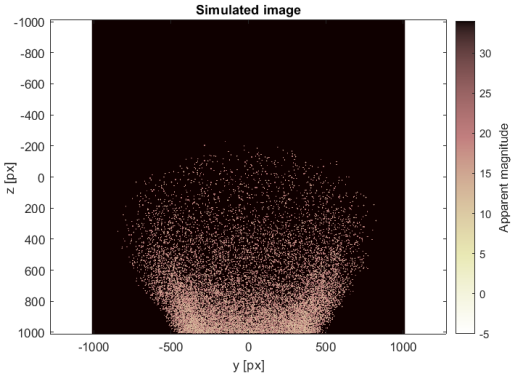

Figure 11: Lander impact simulated image at 20 crater radii form the uncertainty zone. Impact at 45° latitude and 180° longitude, 5 minutes after impact.

As it is possible to observe, in this model, the lander is unable to observe the point of impact. From the images, it can be deduced that the lander can be a useful close observer for the purpose. Implementing a seismograph and other instruments necessary for a complete study of the impact event, a nanolander has the potential to be a good choice in order to obtain the information necessary for the purpose of the mission, without exaggerated development costs, given the evidence of use in the Hayabusa2 mission.

7. Conclusions

The aim of this thesis is the observability model development for small impact on an asteroid, observed from a camera close to the asteroid itself. The study of the image obtained is also preliminary carried forward, especially as regards the total brightness of the image with respect to the position of the observer. Furthermore, the images obtained from a lander positioned close to the impact try to demonstrate their utility for the study of the event, as well as for the study of the internal structure of the asteroid. Observation from the ground is possible, as seen from the simulated images, even at great distances for the safety of the lander itself. The use of the gravitational field coefficient J_4 in the motion equations is certainly of great importance, as explained in [5], with respect to the development of a more realistic model. Furthermore, the image acquisition model proved to be computationally well constructed and effective in target observation.

8. Acknowledgements

I would like to acknowledge and thanks my thesis advisor, Dr. Camilla Colombo, and my thesis co-advisor, Dr. Mirko Trisolini of the Aerospace Science and Technology Department at Politecnico di Milano.

References

[1] Eugene G Fahnestock, Andrew F Cheng, Stavro Ivanovski, Patrick Michel, Sabina D Raducan, Alessandro Rossi, Paul A Abell, Steven Chesley, Elisabetta Dotto, Fabio Ferrari, et al. Pre-encounter predictions of dart impact ejecta behavior and observability. *The Planetary Science Journal*, 3(9):206, 2022.

[2] CW Hergenrother, C Maleszewski, J-Y Li, M Pajola, SR Chesley, AS French, AB Davis, JY Pelgrift, JM Leonard, F Shelly, et al. Photometry of particles ejected from active asteroid (101955) bennu. *Journal of Geophysical Research: Planets*, 125(9):e2020JE006381, 2020.

[3] Kevin R Housen and Keith A Holsapple. Ejecta from impact craters. *Icarus*, 211(1):856–875, 2011.

[4] K Ishibashi, K Shirai, K Ogawa, K Wada, R Honda, M Arakawa, N Sakatani, and Y Ikeda. Performance of hayabusa2 dcam3-d camera for short-range imaging of sci and ejecta curtain generated from the artificial impact crater formed on asteroid 162137 ryugu (1999 ju 3 ju_3). *Space Science Reviews*, 208:213–238, 2017.

[5] Shota Kikuchi, Yusuke Oki, and Yuichi Tsuda. Frozen orbits under radiation pressure and zonal gravity perturbations. *Journal of Guidance, Control, and Dynamics*, 44(11):1924–1946, 2021.

[6] Alexander V Krivov, Miodrag Sremčević, Frank Spahn, Valeri V Dikarev, and Konstantin V Kholshevnikov. Impact-generated dust clouds around planetary satellites: spherically symmetric case. *Planetary and Space Science*, 51(3):251–269, 2003.

[7] Caroline Lange, Jens Biele, Stephan Ulamec, Christian Krause, Barbara Cozzoni, Oliver Küchemann, Simon Tardivel, Tra-Mi Ho, Christian Grimm, Jan Thimo Grundmann, et al. Mascot2–a small body lander to investigate the interior of 65803 didymos moon in the frame of the aida/aim mission. *Acta Astronautica*, 149:25–34, 2018.

[8] Caroline Lange, Tra-Mi Ho, Christian D Grimm, Jan T Grundmann, Christian Ziach, and Roy Lichtenheldt. Exploring small bodies: Nano-and microlander options derived from the mobile asteroid surface scout. *Advances in Space Research*, 62(8):2055–2083, 2018.

[9] Alessandro Latino. Ejecta orbital and bouncing dynamics around asteroid ryugu. *master thesis in Space Engineering at Politecnico di Milano, Supervisor: Camilla Colombo, Co-Supervisors: Dr. Stefania Soldini, Prof. Yuichi Tsuda*, 2019.

[10] James E Richardson, H Jay Melosh, Carey M Lisse, and Brian Carcich. A ballistics analysis of the deep impact ejecta plume: Determining comet tempel 1's gravity, mass, and density. *Icarus*, 191(2):176–209, 2007.

[11] M Trisolini, C Colombo, Y Tsuda, et al. Sensitivity analysis of asteroid ejecta models for future in-orbit sample collection mission. In *INTERNATIONAL ASTRONAUTICAL CONGRESS: IAC PROCEEDINGS*, pages 1–13, 2022.

[12] Eugene Michael Vallerie. Investigation of photometric data received from an artificial earth satellite. Technical report, AIR FORCE INST OF TECH WRIGHT-PATTERSON AFB OH, 1963.

[13] Seiichiro Watanabe, M Hirabayashi, N Hirata, Na Hirata, R Noguchi, Y Shimaki, H Ikeda, E Tatsumi, M Yoshikawa, S Kikuchi, et al. Hayabusa2 arrives at the carbonaceous asteroid 162173 ryugu—a spinning top–shaped rubble pile. *Science*, 364(6437):268–272, 2019.